EGTRIB Journal
JOURNAL OF
THE EGYPTIAN SOCIETY OF TRIBOLOGY
VOLUME 18, No. 2, April 2021, pp. 50 - 62 **ISSN 2090 - 5882**
(Received February 27. 2021, Accepted in final form March 22. 2021) **jest.journals.ekb.eg**

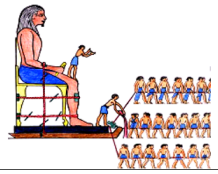

EFFECTS OF DESIGN AND OPERATING PARAMETERS ON HANDLING BEHAVIOR OF A THREE-WHEEL VEHICLE

Gharra F. A.[1], Abdel-Aziz A. I.[1] and Abu-El-Yazied T. G.[2]

[1]Automotive Engineering Department, Faculty of Engineering, Ain Shams University, Cairo, Egypt.
[2] Department of Design and Production Engineering, Faculty of Engineering, Ain Shams University, Cairo, Egypt.

ABSTRACT
Active camber control system is very promising method for handling performance improvement specially for three wheels vehicles. This paper is the first part of a comprehensive study related to the development of a suspension control system applied to a tadpole vehicle utilizing active camber control system. The effect of the vehicle configuration is studied, as well as slip angle effect on vehicle dynamics. Matlab/Simulink ride/handling models including viscus damping and coulomb friction are established to study the effect of changing the camber angle and wheel steering inputs on different vehicle handling parameters. The results showed noteworthy improvement for yaw angle response, rollover, and lateral acceleration threshold. Notable stable and safer cornering performance proved to be achievable.

KEYWORDS
Automotive, Handling, Active suspension, Variable geometry, Camber control, Viscus damping, Coulomb friction, Three wheels vehicle, Rollover threshold, Lateral acceleration threshold.

INTRODUCTION
Traffic problems and expected rising of the fuel cost, drive the need to design light and small vehicles, which, is the current challenge to automotive industry as well as to the R&D engineers. In fact, the awareness for such challenge has been strongly growing up for some time. Further, global warming and the rising screams for lowering air pollution made the EU Environment Agency to set targets to reducing overall cars emissions in 2015 to 130 [g CO_2/km], which have been achieved, and 95 [g CO_2/km] by 2021. New targets were set for 2025 and 2030 as 15% ND 37.5% reductions, repetitively based on 2021 CO_2 emission level [1].

Due to low fuel consumption of the three wheeled cars, they could be very effective and a magic solution to the growing problems. Three wheels vehicles satisfy these needs as being small, having low emissions, and low fuel consumption due to their light weight and low aerodynamic drag, but they have major stability drawback, particularly during cornering.
When the car is cornering at high speed, the resulting centrifugal force tends to alter the car stability causing side skid or even tipping it over in some cases.

To improve the cornering stability, many methods are being applied. Road cambering (Superelevation) is one of the important methods to take in consideration during designing roads [2,3]. It helps to incline the vehicle to counteract the centrifugal force effect. The speed limit, is another method, helps to prevent losing control on the vehicles while turning. Away from external

assist and regulations to avoid problems and accidents, many efforts have been done to develop the passive suspension to achieve more safe vehicles with higher ride quality [4-10].
In cornering stability field, active camber control and body tilting mechanism are highly research and development topics due to their promising results [12-16]. Choosing between active camber control or body tilting highly depends on the vehicle usage. If the vehicle is designed for harsh manoeuvring at high speeds, body tilting mechanism control would be preferred. If the vehicle is designed for normal conditions and city drive, camber control would be preferred [17]. Depending on the suspension type, many camber angle control mechanisms were introduced. Nemeth, et all, discussed the camber control mechanism and the control design using McPherson suspension [18]. On the other hand, camber control mechanisms were introduced into double wishbone suspension system due to its simplicity [19-21].

1 VEHICLE MODEL

Bicycle model is often considered as the most simplified vehicle handling model and many theories and research works have been built using such model [11]. Drawbacks of the bicycle model are the negligence of the effects of vehicle suspension associated dynamics and nonlinearity of tires cornering stiffness. Quarter and half car model were often adopted on ride study [22]. Along with the automotive industry rapid development, more complicated 3D full car model simulations including suspension and tire dynamics were investigated [16,23,24]. However, examination of two configurations of 3D models of three-wheel vehicles are given in following.

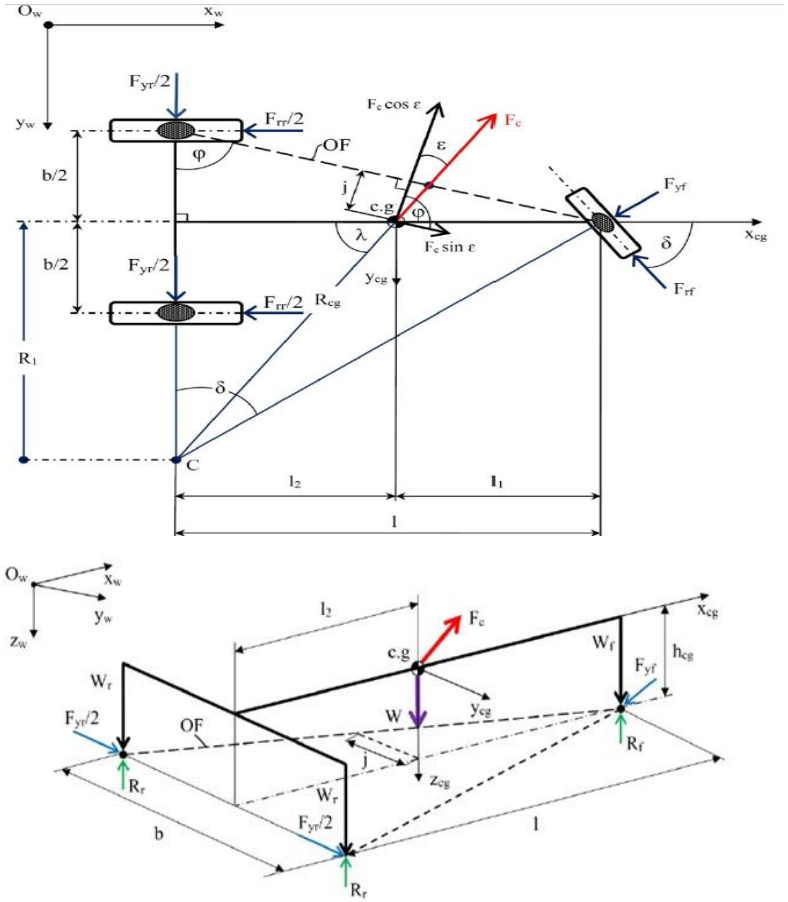

Figure (1) A 3-wheel delta configuration vehicle 3D rollover model [25].

From Figure (1) the following relations are deduced [25].

$$R_1 = \frac{L}{tan\,\delta}\ and\ R_{c.g} = \sqrt{L^2 + R_1^2} \qquad (1)$$

To find the rollover speed, moments about line OF, $\Sigma M_{OF} = 0$ gives: $V_{roll} = \sqrt{\frac{j\, g\, R_{c.g}}{h_{c.g}\, cos\, \varepsilon}}$ (2)

where; $j = \frac{0.5\, b\, l_1}{\sqrt{L^2 + \left(\frac{b}{2}\right)^2}}$, $\varepsilon = \varphi - \lambda$, $\varphi = \frac{2L}{b}$ and $\lambda = \frac{l_2}{Rc.g} = \frac{R1}{l_2}$

2.1 Vehicle Configuration Selection

From the aerodynamics point of view, tadpole body configuration can match the aerofoil shape easily than delta. For braking force distribution, more front capacity is available in case of tadpole than delta. Hence, tadpole configuration is preferred for braking. In tadpole with rear wheel drive, no differential is needed, and a lighter vehicle can be achieved.

To examine the dynamic stability during cornering manoeuvre, the rollover speed is calculated for both configurations and the results are discussed in the following.

2.1.1 Delta Configuration

Figure (1) shows a 3-wheel delta configuration vehicle 3D rollover model. The local vehicle axes, the dynamic forces, the wheel reactions, and the global axes as well as the dimension symbols are shown on the figure. Moreover, the definitions of each symbols are given in the nomenclature table.**2.1.2 Tadpole Configuration**

Figure (2) shows a 3-wheel tadpole configuration vehicle rollover model. The local vehicle axes, the dynamic forces, the wheel reactions, and the global axes are shown on the figures.

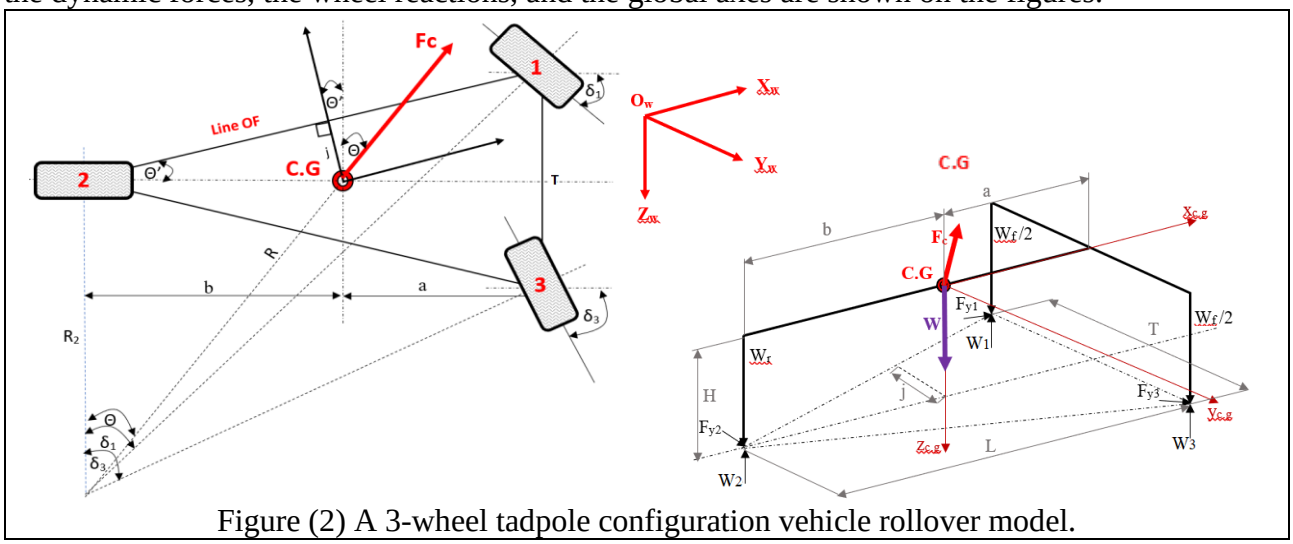

Figure (2) A 3-wheel tadpole configuration vehicle rollover model.

From Figure (2), the following relations are deduced.

$$L = a + b, \qquad R_2 = \frac{L}{tan\ \delta_3} + \frac{T}{2} \quad and \quad R = \sqrt{b^2 + {R_2}^2} \tag{3}$$

To find the rollover speed, moments around line OF, $\Sigma M_{OF} = 0$ gives: $V_{roll} = \sqrt{\frac{j\, g\, R}{H\, cos\, \varepsilon}}$ (4)

where $j = \frac{0.5T\ a}{\sqrt{L^2 + \left(\frac{T}{2}\right)^2}}$, $\varepsilon = \theta + \theta'$, $\theta' = j/b$, $and\ \theta = b/R_2$

Figure (3) shows the variations of rollover speed and the turning radius of c.g. versus steering angle input for both delta and tadpole configuration models. It worth mentioning here that, the wheel track, the wheelbase, height of the c.g. and GVM values are the same for both models. It is obvious

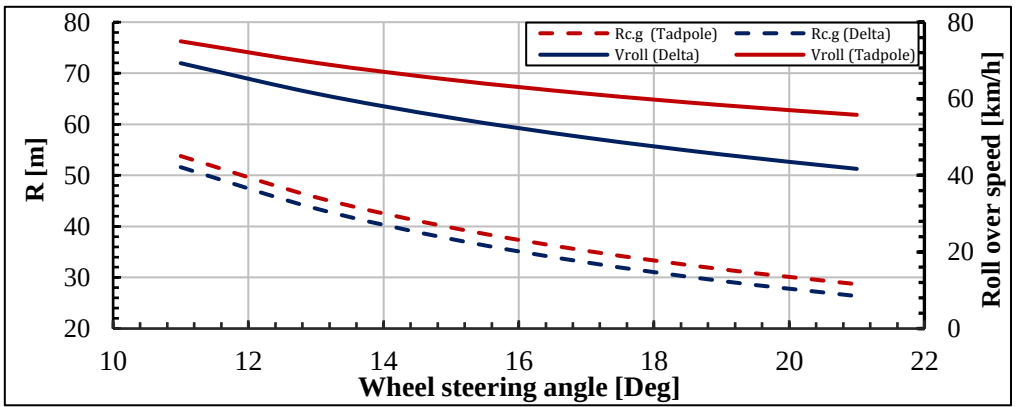

that tadpole V_{roll} has higher values than that of the delta configuration over the range of the steering angle input. The difference increases as the steering angle increases. Therefore, tadpole configuration is more stable in cornering manoeuvres (keeping in mind all hypotheses made for the two models).

Figure (3) Relationship between rollover speed, turning radius vs steering angles for tadpole and delta configurations.

2.2 Model Simplifications

Due to the lateral load transfer, specially at the verge of rollover, the vertical load on the inner front tire diminishes, henceforth its capability to create slip angle. Therefore, α_3 is considered equal to zero.

2.2.1 Slip Angle Calculation

Based on the model shown in Figure (4), front and rear tire slip angle values are calculated at different steering angles for the tadpole configuration.

In triangle OAC.

$$OC = R,\ AC = \sqrt{\left(\frac{T}{2}\right)^2 + a^2}\ \text{, and}\ C\hat{A}O = (90 - \delta_3) + \left(\frac{T/2}{a}\right)$$

From which.

$$Angle\ A\hat{O}C = \left[\frac{sin\,(C\hat{A}O) \times \sqrt{\left(\frac{T}{2}\right)^2 + a^2}}{R}\right]\ ,A\hat{C}O = \left(\pi - C\hat{A}O - A\hat{O}C\right),\ and\ R_3 = \frac{Rsin\,A\hat{C}O}{sin\,O\hat{A}C} \qquad (5)$$

In triangle OAD: $OA = R_3,\ D\hat{A}O = \frac{\pi}{2} - \delta_3 + \psi,\ and\ \ AD = \sqrt{\left(\frac{T}{2}\right)^2 + L^2}$

Hence; $OD = R_2 = \sqrt{AD^2 + {R_3}^2 - 2AD * R_2 \cos\left(D\hat{A}O\right)}$, $O\hat{D}A = \cos^{-1}\left(\frac{{R_2}^2 + AD^2 - {R_3}^2}{2AD * R_2}\right) = \frac{\pi}{2} - \alpha_r - \psi$ (6)

From equation (6) α_r can be obtained.

In triangle ABO: $AB = T\ ,\ AO = R_3$ and $B\hat{A}O = \pi - \delta_3$

Following similar approach $\alpha_f = \alpha_1$ can be obtained from equation (7).

$$R_1 = \sqrt{T^2 + {R_3}^2 - 2TR_3 \cos(B\hat{A}O)}\ , A\hat{B}O = \cos^{-1}\left(\frac{T^2 + {R_1}^2 - {R_3}^2}{2TR_1}\right) = \delta_1 - \alpha_f \qquad (7)$$

As shown in Figure (5), α_f and α_r have small values specially at high cornering radiuses which are more realistic. Moreover, the difference between the two angles is very small and hence can be neglected. Noteworthy, the crossover point occurs at $\delta_f \cong \frac{L}{R}$ which can be considered as optimum steering angle value.

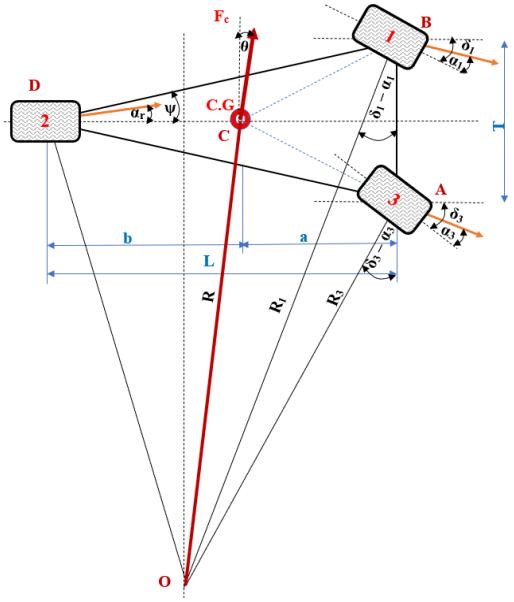

Figure (4) A 3-wheel tadpole configuration vehicle model in x_{cg}-y_{cg} plane**.**

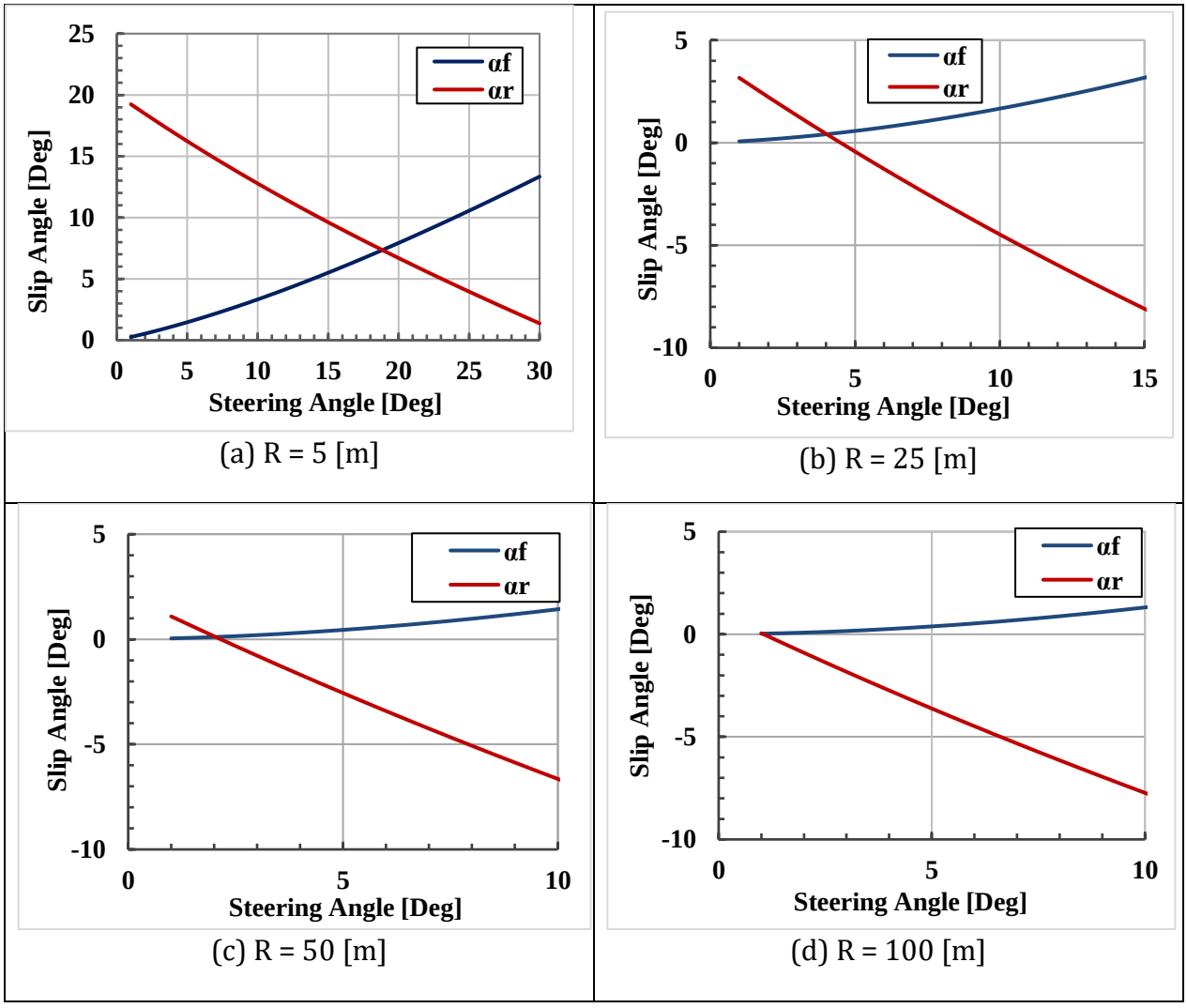

Figure (5) Front and rear wheels slip angles vs Steering angle**.**

2.2.2 Cornering force direction

From Figure (4), the cornering force inclination to vertical axis, ɵ can be obtained as follows.

$$\theta = \frac{\pi}{2} - A\widehat{C}O - \left(\frac{T/2}{a}\right) \quad (8)$$

The cornering force inclination angle was calculated at different steering angle for four road curvature radiuses as shown in Figure (6). The result shows that θ has small value (less than 10°) for steering angle less than 10° and this result is not affected by the curvature radius value. Hence, its proved that the cornering force is almost perpendicular to vehicle x-axis at small steering angle values.

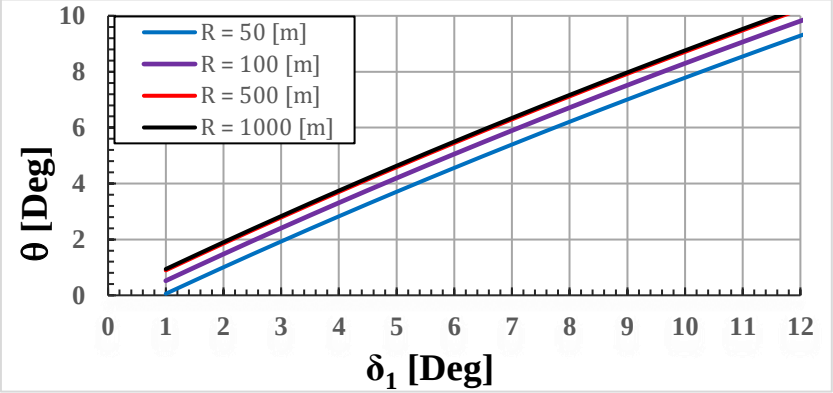

Figure (6) Lateral force direction with vertical axis vs steering angle at different radii.

2.3 Mathematical Model

Full car model was applied with the following simplifications as shown in Figure (7). Tire stiffness coefficient was assumed to be constant (linear tire model), slip angles were neglect, c.g and roll centre were assumed to be at fixed place (ignoring weight transfer), and based on the result on Figure (6), cornering force is assumed to be perpendicular to vehicle x-axis when applying small steering input. The following relations are deduced.

Lateral forces equation:

$$m\,(\dot{V}_y + V_x r) = F_{y1} + F_{y2} + F_{y3}\ \text{, where}\ F_{yn} = \left(C_{\alpha n}\alpha_n + C_{\gamma n}\gamma_n\right) \times \cos\delta_n \quad (9)$$

While Cγ is the cambering stiffness and assumed to equal 0.2 Cα, [11] and δ_n is the steering angle for the tire number (n). The steering is only applied on front wheels so δ_2=0 while the relation between front tires is given by;

$$cot\,(\delta_1) - cot\,(\delta_2) = \frac{B}{L} \quad (10)$$

Where; $\alpha_1 = \delta_1 - \left(\frac{V_y + ar}{V_x}\right)$, $\alpha_2 = \delta_2 - \left(\frac{V_y - br}{V_x}\right)$ *and* $\alpha_3 = \delta_3 - \left(\frac{V_y + ar}{V_x}\right)$ (11)

Yaw equation:

$$I_z\dot{r} = a\left(F_{y1} + F_{y3}\right) - b\,F_{y2} \quad (12)$$

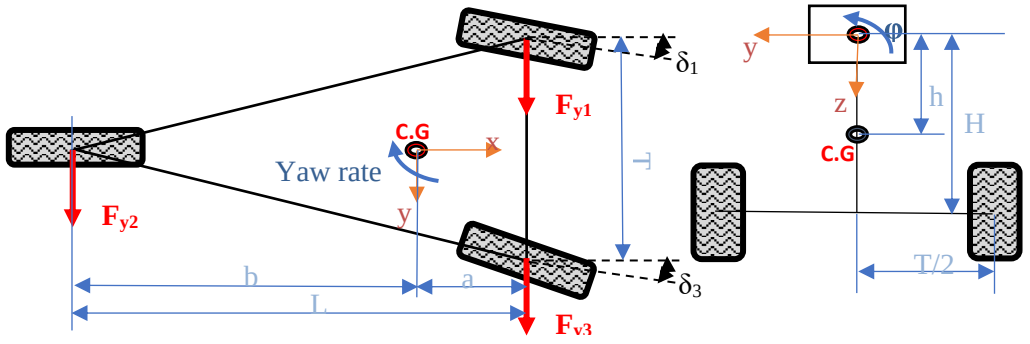

Figure (7) A 3-wheel tadpole vehicle dynamic model in x_{cg}-y_{cg} and z_{cg}-y_{cg} planes [16].

Roll equation:

For the roll mathematical model, 2 models are inspected: (a) linear model and (b) non-linear model with coulomb friction [26, 27] together with different values for the rebound and compression damping coefficients.

(a) Linear roll equation:

$$I_x\ddot{\varphi} + C_t\dot{\varphi} + (K_t - m_s gh)\varphi = -m_s h\,(\dot{V}_y + V_x r) \quad (13)$$

Figure (8) shows spring and damper forces direction so the following equations can be deduced.

$$F_{sp} = K_{sp} \times d \quad , \quad F_d = C_{sp} \times d' \quad (14)$$

Where; $d = \frac{T}{2} \times sin\,(\emptyset)$,and $d = \frac{T}{2} \times \emptyset \quad , \quad d' = \frac{T}{2} \times \dot{\emptyset}$

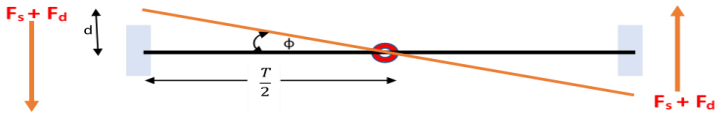

Figure (8) Spring and Damper Forces direction.

The spring and damper moments can be deduced as follows.

$$M_s = F_{sp} \times \frac{T}{2} + F_{sp} \times \frac{T}{2} = F_{sp} \times T = \frac{T^2}{2} \times K_{sp} \times \emptyset \quad (15)$$

$$M_d = F_d \times \frac{T}{2} + F_d \times \frac{T}{2} = F_d \times T = \frac{T^2}{2} \times C_{sp} \times \dot{\emptyset} \quad (16)$$

Where; $K_t = \frac{T^2}{2} \times K_{sp}, \quad C_t = \frac{T^2}{2} \times C_{sp}$

(b) *Non-linear roll equation. with Coulomb friction* [26, 27]

$$I_x\ddot{\varphi} + C_c L \times \frac{L}{2}\dot{\varphi} + C_r L * \frac{L}{2}\dot{\varphi} + \mu f_{sus} L\dot{\varphi} + {K_s}^n L\varphi + (K_t - m_s gh)\varphi = -m_s h\,(\dot{V}_y + V_x r) \quad (17)$$

And by assuming that $C_r = 2.5\,C_c$, then;

$$I_x\ddot{\varphi} + C_c \frac{3.5L^2}{4}\dot{\varphi} + \mu f_{sus} L\dot{\varphi} + {K_s}^n L\varphi^3 + (K_t - m_s gh)\varphi = -m_s h\,(\dot{V}_y + V_x r) \quad (18)$$

Where;

- C_c; Compression damping stiffness and C_r: rebound damping stiffness.
- μ; Coulomb friction constant and is taken equal 1.
- f_{sus}; fraction from the sprung mass weight =$0.1M_s \times g$.
- ${K_s}^n$; nonlinear stiffness coefficient.

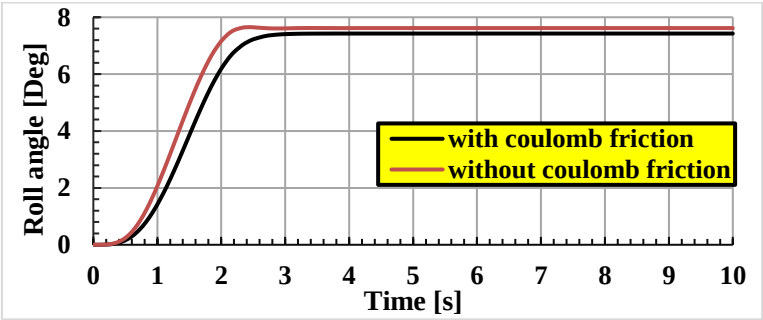

Figure (9) Coulomb friction addition effect on roll angle.

Figure (9) shows that the roll angle reaches steady state value of 7.624° in case of applying linear roll equation, Equation (13), while in case of applying non-linear roll equation by adding the coulomb friction consideration, Equation (18), the steady state is reached at 7.424° which gives 2.6% error, then the coulomb friction effect can be neglected.

Lateral acceleration threshold

Two cases of camber angle control are studied, the first one is controlling all wheel angles, while the second one is considered as special case from the first one, where only front wheels are controlled. Figure (10) shows Changes upon applying camber angle to three wheels. As shown, the most important direction parameters for improving lateral acceleration are outer wheel leaning towards the turn and the rear wheel leaning outward the turn to maximise the parameter h". The inner wheel has zero load in case of tipping over, then its leaning direction has no impact. From figure (10) the following equations can be deduced.

$$\theta_1 = \left(\frac{\frac{T}{2} + r\sin(\gamma_1)}{L+K}\right), K = \frac{r\sin\gamma_2}{\tan\theta_1} = \frac{2Lr\sin\gamma_2}{T + 2r(\sin\gamma_1 - \sin\gamma_3)}, \qquad q = h \times \sin(\emptyset)$$

$$, h'' = (b+K)\sin\theta_1 = \frac{b\,(T+2r\,\sin\sin\gamma_1)}{2(L+K)}\cos\theta_1 \text{ , and}$$

$$p = h\,(1 - \cos(\emptyset)) + \frac{b}{L} \times \left[\frac{1}{2}\,r\,\left((1-\cos\gamma_3) + (1-\cos\gamma_1)\right)\right] + r(1-\cos\gamma_2) \qquad (19)$$

To calculate the lateral acceleration threshold due to the new suspension geometric change, the moment about rollover axis is applied.

$$[mg * (h'' - q)] - \left[\left(ma_y\cos\theta_1 - ma_x\sin\theta_1\right) * (H-p)\right] = 0 \qquad (20)$$

From equations (19 & 20) Then;

$$a_y = \frac{(T+2r\,\sin\gamma_1)(b+K)g\cos\theta_1 - 2(L+K)hg\,\sin\emptyset}{2(L+K)\cos\theta_1 * \left[H - h\,(1-\cos(\emptyset)) - \frac{b}{L}*\left[\frac{1}{2}r\,\left((1-\cos\gamma_3)+(1-\cos\gamma_1)\right)\right] - r(1-\cos\gamma_2)\right]} + \frac{ax\,\sin\theta_1}{\cos\theta_1} \qquad (21)$$

Where ϕ is the threshold yaw angle and from Equation (13), it can be given by; $|\emptyset_{th}| = \frac{m\,a_y h}{(mgh - K_t)}$

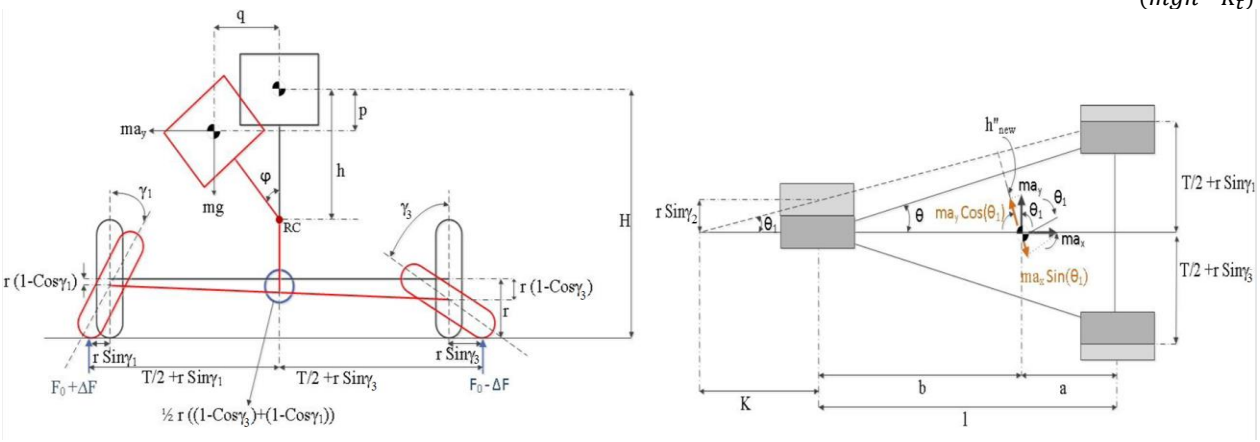

Figure (10) Changes upon applying camber angle to three wheels [16].

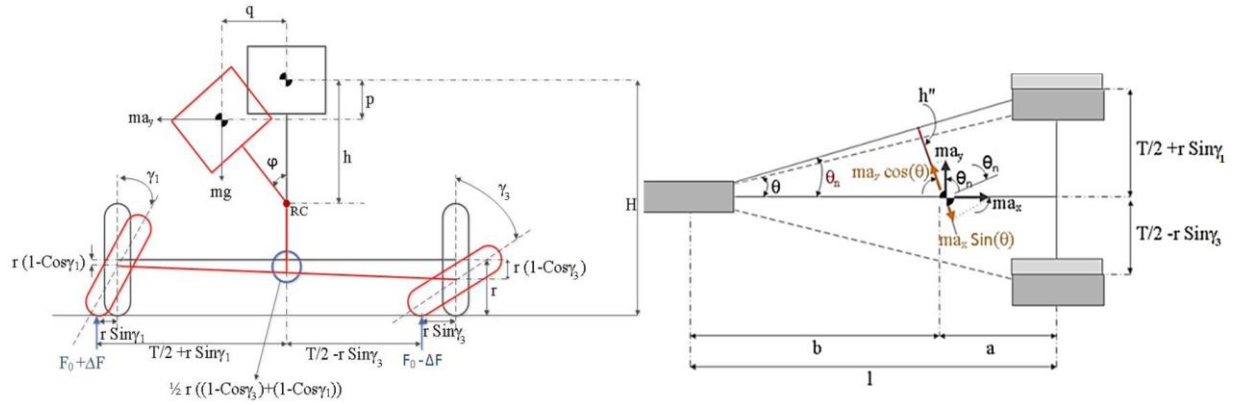

Figure (11) Changes upon applying one positive and one negative camber angle to the front wheels [16].

Figure (11) shows case two where one positive and one negative camber angle when applied to the front wheels. As mentioned before the inner wheel angle sign is not important when studying rollover threshold. Hence, by setting the rear wheel camber angle, γ_2 to zero at equation (21), The lateral acceleration threshold can be determined by equation (22).

$$a_y = \frac{(T+2r\sin\gamma_1)bg\cos\theta_n - 2Lhg\sin\emptyset}{2L\cos\theta_n \times \left[H - h\,\{1-\cos(\emptyset)\} - \frac{br}{2L}\times[2-\cos\gamma_3 - \cos\gamma_1]\right]} + \frac{a_x\,\sin\theta_n}{\cos\theta_n} \qquad (22)$$

3 CASE STUDY

Steering wheel input δ_1 and camber angle with 2 seconds time lag between applying them are considered as main time variant inputs to the model as shown in Figure (12).

A constant 50 [m] turning radius is considered during the study. Moreover, another studying criteria is the C.G height effect. The results were plotted at 2 different H values, H = 0.5 [m] and H = 0.6 [m].

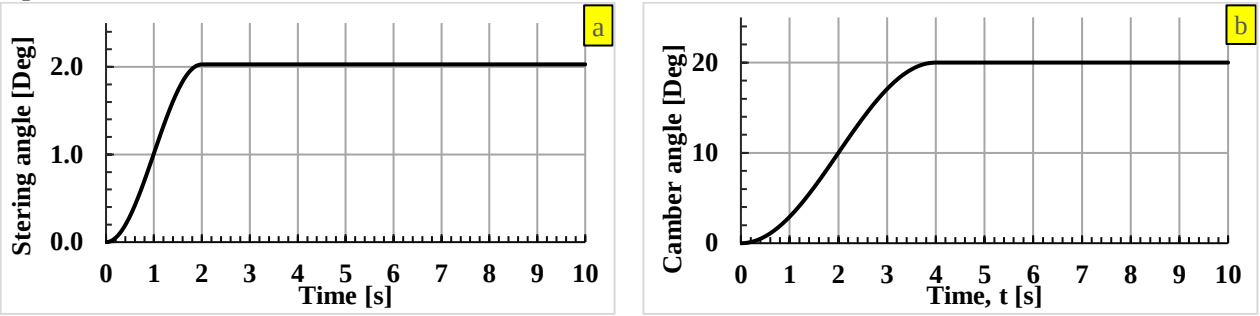

Figure (12) Steering input δ_1 vs time (a) and camber angle γ_1 vs time (b).

2 SIMULATION RESULTS

Tables (1 and 3) show how camber angle improves the vehicle lateral acceleration threshold for both studying cases, H = 0.5 [m] and H = 0.6 [m]. However, lateral acceleration has maximum limit depending on side skid threshold. Hence, lateral acceleration threshold must be equal or below the skid limit to be applicable. γ_1 and γ_3 are front wheels camber angle, and they are assumed to have equal values and direction to produce camber thrust to resist the centrifugal force, while γ_2 is the rear wheel camber angle. The negative sign of camber angle values refers to that the rear wheel should lean outward the turning path to cause improvement as previously mentioned. The maximum speed is also calculated based on 50 [m] turning radius according to the following relation $a_y = V^2/R$.

Tables (2 and 4) show the cases which fulfils a 50 [m] turning radius, noted that when only front wheels are cambered, they have a steering effect, while in case of all wheels cambered the steering effect vanishes. The yellow shaded cases are the chosen cases to be investigated.

Table (1) Lateral acceleration threshold for different camber angle values at H 0.5 [m].

$\gamma_1{}^o$	$\gamma_3{}^o$	$\gamma_2{}^o$	Lateral acceleration Threshold in g unit	Side Skid Threshold	Improvement Percentage	Vmax in [km/h] for R= 50 [m]
0	0	0	0.73	0.8 g	0	68.25
+5	+5	0	0.76		3.60	69.50
+10	+10	0	0.79		7.50	70.77
+15	+15	0	0.82		9.04	71.30
+20	+20	0	0.85		9.04	71.3
+5	+5	-5	0.78		7.40	70.73
+10	+10	-10	0.85		9.04	71.30
+15	+15	-15	0.91		9.04	71.30
+20	+20	-20	0.98		9.04	71.30

Table (2) Maximum speed for different study cases at H = 0.5 [m].

Case	V [km/h]	δ_1 °	$\gamma_1{}^o$	$\gamma_3{}^o$	$\gamma_2{}^o$
1	68.3	2.03	0	0	0
2	69.5	1.05	+5	+5	0
3	70.8	0.06	+10	+10	0
4	71.3	0	+10.3	+10.3	0
5	70.7	2.03	+5	+5	-5
6	71.3	2.03	+10	+10	-10
7	71.3	2.03	+15	+15	-15
8	71.3	2.03	+20	+20	-20

Table (3) Lateral acceleration threshold for different camber angle values at H = 0.6 [m].

γ_1^o	γ_3^o	γ_2^o	Lateral acceleration Threshold in g unit	Side Skid Threshold	Improvement Percentage	Vmax [km/h] R= 50 [m]
0	0	0	0.58	0.8g	0	60.6
+5	+5	0	0.60		3.7	61.7
+10	+10	0	0.62		7.4	62.8
+15	+15	0	0.64		11.3	63.9
+20	+20	0	0.67		15.3	65.1
+5	+5	-5	0.62		6.9	62.8
+10	+10	-10	0.66		14.9	64.9
+15	+15	-15	0.71		23.3	67.3
+20	+20	-20	0.77		32.4	69.8

Table (4); Maximum speed for different study cases at H = 0.6 [m].

Case	V [km/h]	δ_1 °	γ_1^o	γ_3^o	γ_2^o
Case 1	60.6	2.03	0	0	0
Case 2	62.8	0	+10.3	+10.3	0
Case 3	69.8	2.03	+20	+20	-20

Figure (13) shows lateral acceleration threshold taking in consideration the skidding threshold. As seen in case of H = 0.5 [m], which is more stable vehicle, small camber angles can be applied, while for H = 0.6 [m] a 20^o camber angle applied to all wheels can be applied to improve lateral acceleration threshold. Moreover, if the hydraulic actuator can afford higher camber angle, it can be applied to achieve higher lateral acceleration threshold.

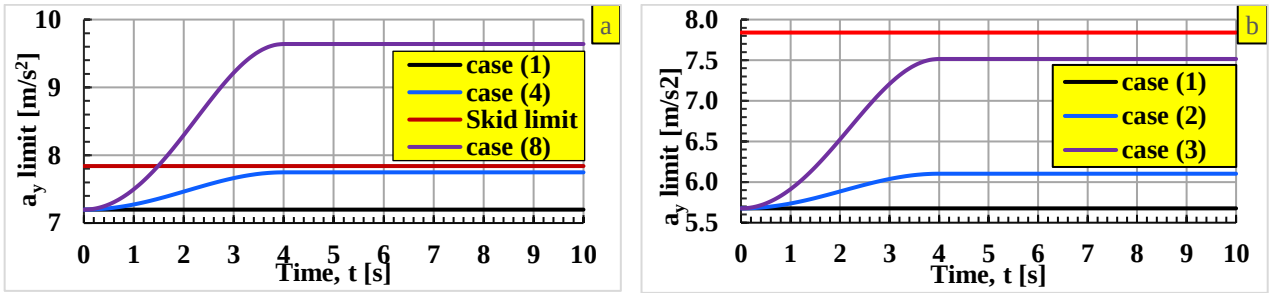

Figure (13) Lateral acceleration threshold vs time at (a) H= 0.5 [m] and (b) H = 0.6 [m].

Figures (14-16) shows roll angle, lateral acceleration, and yaw rate vs time for all the studied cases. The camber angle control system shows overall handling performance improvement. In case of H = 0.5 [m], case 4 and case 8 gives the same steady state improvement as both reach the ultimate lateral acceleration threshold. While for transient roll angle and lateral acceleration responses, case 4 reaches the steady state without overshoot as in case of case 8.

For yaw rate response, no overshoot occurs at both cases but it worth mentioning that case 8 reached steady state 2 seconds faster than case 4. The camber angle control effect is more obvious in case of H = 0.6 [m] than H = 0.5 [m]. The performance is improved as the camber angle increases specially when all wheels are cambered.

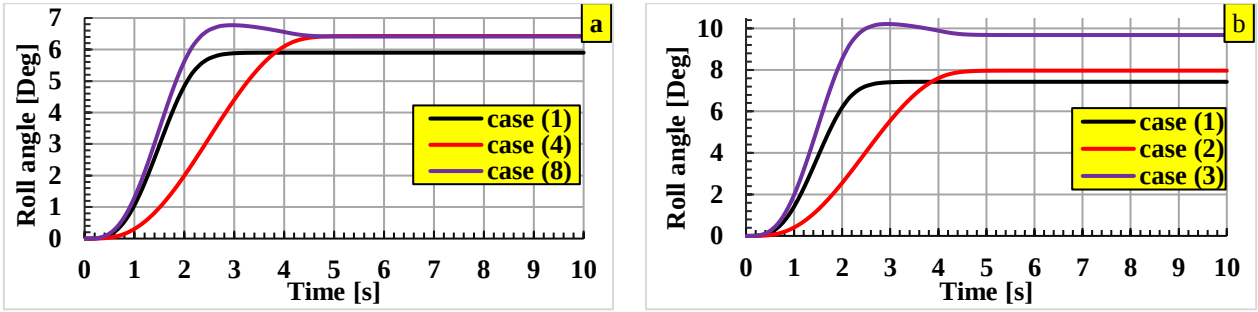

Figure (14) Roll angle vs time at (a) H= 0.5 [m] and (b) H = 0.6 [m].

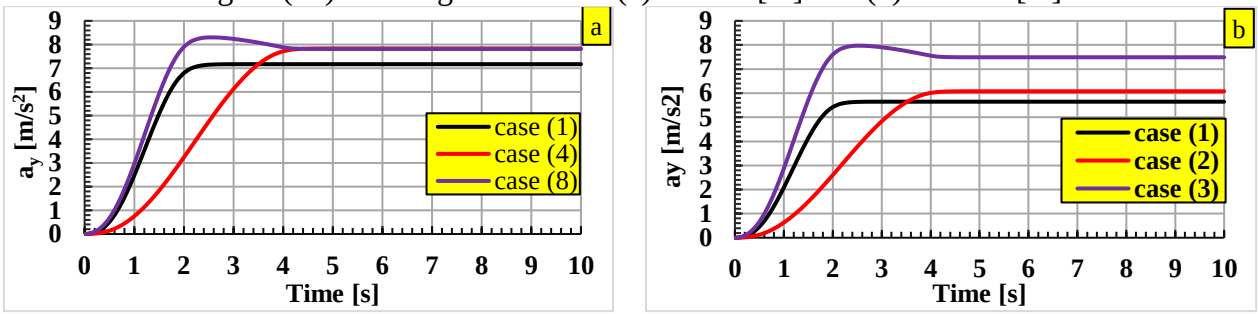

Figure (15) Lateral acceleration vs time at (a) H= 0.5 [m] and (b) H = 0.6 [m].

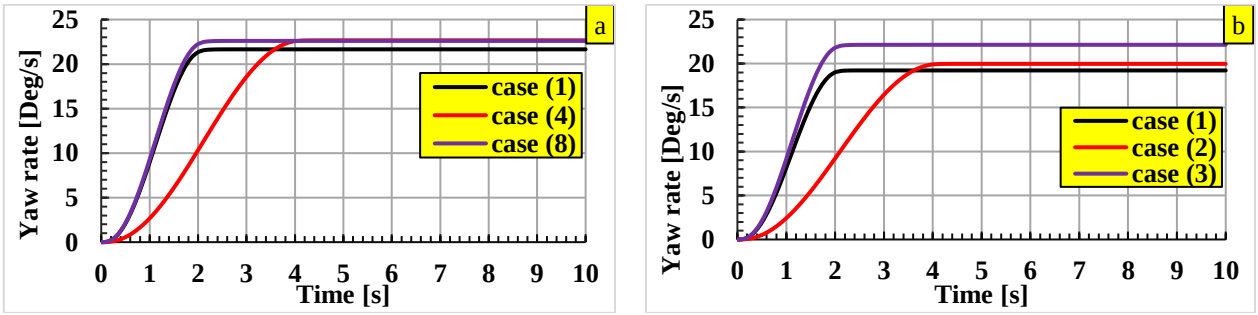

Figure (16) Yaw rate vs time at (a) H= 0.5 [m] and (b) H = 0.6 [m].

CONCLUSIONS

- Tadpole configuration is more stable in cornering performance.
- The difference between α_f and α_r is very small, hence can be neglected especially for low steering angle input.
- The cornering force is almost perpendicular to vehicle x-axis at small steering angle values.
- Only 2.6 % error in roll angle value was obtained when adding coulomb friction, then the effect of the coulomb friction can be neglected.
- The inner wheel has no road reactions at the verge of rollover, then its leaning direction has no impact.
- To improve lateral acceleration, outer wheels should be leaning towards the turn, while the rear wheel should be leaning outward the turn.
- When only front wheels are cambered, they have a camber steering effect, while in case of all wheels cambered the steering effect diminishes.
- The handling performance in terms of rollover speed is improved as the camber angle increases specially when camber control is applied to all wheels. Lateral acceleration threshold is increased as camber angle increases but the skidding threshold should be taken into consideration.

Nomenclature

Symbol	Description	Symbol	Description

a	Front axle distance to C.G	R	C.G turning radius
b	Rear axle distance to C.G	r	Yaw velocity (rate)
C_c	Compression damping stiffness	R_n	Wheel (n) turning radius
C_r	Rebound damping stiffness.	T	Vehicle track
C_{sp}	Damping coefficient	V_{roll}	Rollover speed
$C_{\alpha n}$	Wheel (n) cornering stiffness	Vx	Longitudinal velocity
$C_{\gamma n}$	Wheel (n) cambering stiffness	V'_x	Longitudinal acceleration
F_d	Damping force	V_y	Lateral Velocity
F_{sp}	Spring force	V'_y	Lateral acceleration
f_{sus}	fraction from the sprung	αf	Outer front tire slip angle
F_{yn}	Wheel (n) cornering force	α_n	Wheel (n) slip angle
g	Gravitational acceleration	αr	Rear tire slip angle
h	C.G height from the roll centre	γ_n	Wheel (n) camber angle
H	Distance between C.G and ground	δ_n	Tire (n) steering angle
Ix	Moment of inertia about x- axis	ε	Angle between the cornering force and the perpendicular direction of the rollover axes
j	Perpendicular distance between C.G and the rollover axis	θ	Vertical inclination of the cornering force
K_s^n	nonlinear stiffness coefficient.	θ'	Vertical inclination the perpendicular direction of the rollover axes
K_{sp}	Spring stiffness	λ	Horizontal inclination of the line between C.G and centre of rotation
L	Wheelbase	μ	Coulomb friction constant
m	Vehicle mass	φ	Vertical inclination of the rollover axes
m_s	Vehicle sprung mass	φ	Roll angle
m_{us}	Vehicle unsprung mass	$\dot{\varphi}$	Roll angle velocity
p	Vertical C.G shift	$\ddot{\varphi}$	Roll angle acceleration
q	Horizontal C.G shift	ψ	Horizontal inclination of the rollover axes

REFERENCES

1. Technical report, European Environment Agency, "Monitoring CO_2 emissions from new passenger cars and vans in 2017", No 15/2018.
2. Azad Abdulhafedh, "Design of Superelevation of Highway Curves: An Overview and Distribution Methods", Journal of City and Development, Vol. 1, No. 1, 35-40, 2019.
3. A policy on "Geometric Design of Highways and Streets", American Association of State Highway and Transportation Officials, Fifth edition, 2004.
4. R. S. Sharp and D. A. Crolla, "Road vehicle suspension system design- a review," Vehicle System Dynamics, vol. 16, no. 3, pp. 167–192,1987.
5. X. D. Xue, K. W. E. Cheng, Z. Zhang, J. K. Lin, D. H. Wang, Y. J. Bao, M. K. Wong, and N. Cheung, "Study of Art of Automotive Active Suspensions", 4th International Conference on Power Electronics Systems and Applications, 360-366, 2011.
6. D. Karnopp, "Theoretical limitations in active vehicle suspensions," Vehicle System Dynamics, vol. 15, no. 1, pp. 41–54, 1986.
7. E. K. Bender, "Optimal linear preview control with application to vehicle suspension," in: Trans. ASME J. Basic Eng., vol. 90, no. 2, pp. 213-221, 1968.
8. R. G. Langlois, R. J. Anderson, and D. M. Hanna, "Implementing preview control on an off-road vehicle with active suspension," Proc. of 12th IAVSD Symposium on the Dynamics of Vehicles, 1992.
9. Mahmoud Ahmed and Ferdinand Svaricek, "Preview Control of Semi-active Suspension Based on a Half-car Model Using Fast Fourier Transform", 10th International Multi-Conference on Systems, Signals & Devices (SSD) Hammamet, Tunisia, March 2013.

10. Ayman A. Aly, El-Shafei Zeidan, Ahmed Hamed, and Farhan Salem, “An Antilock-Braking Systems (ABS) Control: A Technical Review”, Journal of Scientific Research, pp. 186-195, 2011.
11. J. Y. Wong, “Theory of Ground Vehicle”, 3rd edition, 2001.
12. Balazs Nemeth and Peter Gaspar, “Set-based analysis of the variable-geometry suspension system”, Proceedings of the 19th World Congress, The International Federation of Automatic Control, Cape Town, South Africa, 2014.
13. Takahiko Yoshino, Hiromichi Nozaki, “Active Control Method for Critical Cornering Range”, Journal of Society of Automotive Engineers of Japan, http://dx.doi.org/10.4236/eng.2014.68043, 2014.
14. Takahiko Yoshino, Hiromichi Nozaki, “Camber Angle Control Method Corresponding to the Electric Vehicle Age”, Journal of Society of Automotive Engineers of Japan, http://dx.doi.org/10.4236/eng.2014.68049, 2014.
15. Shinji Kajiwara, “New Suspension Mechanism Using Camber Thrust for a Formula Car”, World Academy of Science, Engineering and Technology, International Journal of Mechanical, Aerospace, Industrial, Mechatronic and Manufacturing Engineering Vol:8, No:2, 2014.
16. Azadeh Zandieh, “Dynamics of a Three-Wheel Vehicle with Tadpole Design”, degree of Master of Science in Mechanical Engineering, University of Waterloo, 2014.
17. Johan J. H. Berote, “Dynamics and Control of a Tilting Three Wheeled Vehicle”, degree of Doctor of Philosophy, The University of Bath, 2010.
18. Balazs Nemeth, Daniel Fenyesm and Peter Gaspar, “Independent wheel steering control design based on variable-geometry suspension”, 8th IFAC Symposium on Advances in Automotive Control AAC 2016: Norrköping, Sweden, 20-23 June 2016.
19. Isao Kuwayama, Fernando Baldoni, Fedelico Cheli, “A Full Vehicle Model for The Development of a Variable Camber Suspension”, The ASME International Design Engineering Technical Conferences & Computers and Information in Engineering Conference IDETC/CIE, Las Vegas, Nevada, USA, September 2007.
20. Seong-Jun Park and Jeong-Hyun Sohn, “Effects of Camber Angle Control of Front Suspension on Vehicle Dynamic Behavior”, Journal of Mechanical Science and Technology, 26 (2), P 307-313, 2012.
21. M.I.K Esfahani, M. Mosayebi, M. Pourshams, A. Keshavarzi, “Optimization of Double Wishbone Suspension System with Variable Camber Angle by Hydraulic Mechanism”, World Academy of Science, Engineering and Technology, vol 61, pp. 299-306, 2010.
22. Jay E. Shannan, “Ride and handling models of a vehicle with active suspensions”, Master of Science Thesis, Iowa State University, 1986.
23. Syabillah Sulaiman, Pakharuddin M. Samin, Hishamuddin Jamaluddin, Roslan Abd Rahman, and Mohammad S. Burhaumudin, “Modeling and Validation of 7-DOF Ride Model for Heavy Vehicle”, International Conference on Automotive, Mechanical and Materials Engineering (ICAMME'2012), Penang, Malaysia, May 2012.
24. M.K Naidu, S Srinivasa Rao and T Tejesh, “Ride Analysis of Three Wheeled Vehicle Using MATLAB/Simulink”, AMAE Int. J. on Manufacturing and Material Science 2012, Vol. 02, No. 01, May 2012.
25. M.T. Heshmat, “Dynamic Performance of a Three-Wheeled Vehicle Steering System, Part 2: Steer by Wire and Vehicle Dynamics during Steering”, Proceedings of the 15th international conference on aerospace sciences & aviation technology, 2013.
26. Ozgur Demir, lknur Keskin, and Saban Cetin, “Modeling and control of a nonlinear half-vehicle suspension system: a hybrid fuzzy logic approach”, Springer Science, Business Media B.V., 2011.
27. McGee, C.G., Haroon, M., Adams, D.E.,and Luk, Y.W., “A frequency domain technique for characterizing nonlinearities in a tire-vehicle suspension system” J. Vib. Acoust. 127, 61–76 (2005), 2005.